# Revision 1

# Thermodynamics of Bastnaesite - a Major Rare Earth Ore Mineral

**Radha Shivaramaiah[1], Andre Anderko[2], Richard E. Riman[3] and Alexandra Navrotsky[1,*]**

[1]Peter A. Rock Thermochemistry Laboratory and NEAT ORU, University of California Davis, Davis, CA 95616, USA

[2]OLI Systems, Inc. 240 Cedar Knolls Road, Cedar Knolls NJ 07927, USA

[3] Department of Materials Science and Engineering, The State University of New Jersey, Piscataway, NJ 08854-8066, USA

## Abstract

Bastnaesite, [RE-$CO_3$-OH/F] (RE = rare earth) is one of the major sources of rare earth elements found in commercial deposits at Mountain Pass, California, Bayan Obo, China, and elsewhere. Synthetic forms of bastnaesite have been explored for applications including optical devices and phosphors. Determination of thermodynamic properties of these phases is critical for understanding their origin, mining, and processing. We report the first experimental determination of formation enthalpies of several OH and F bastnaesites based on high temperature oxide melt solution calorimetry of well characterized synthetic samples. The formation enthalpies from binary oxides and fluorides for all the bastnaesite samples are highly exothermic, consistent with their stability in the garnet zone of the Earth's crust. Fluoride bastnaesite, which is more abundant in nature than its hydroxide counterpart, is thermodynamically more stable. For both OH and F bastnaesite, the enthalpy of formation becomes more negative with increasing ionic radius of the $RE^{3+}$ cation. This periodic trend is also observed among rare earth phosphates and several other rare earth ternary oxides. For a given RE, the formation enthalpies from binary oxides are more negative for orthophosphates than for bastnaesites, supporting the argument that monazite could have formed by reaction of bastnaesite and apatite at high temperature. The difference in formation enthalpy of monazite and bastnaesite provides insight into energetics of such reactions along the rare earth series.

## Introduction

Rare earth elements (RE) are technology drivers in today's world where they are integrated into every part of modern military and civilian life, including rechargeable batteries and other energy applications, phosphors for lighting and computer displays, catalytic converters, and magnets (McLellan et al. 2013; Pathak et al. 2015; Gschneider 1981). Their wide application has created a high demand, which makes their availability a crucial issue, or, in other words, a critical material (Alonso et al. 2012; Humphries 2010). REs occur in nature both as major and trace constituents of minerals (Keith 2011). Monazite, bastnaesite, xenotime, aeschynite and allanite are minerals in which RE is an essential constituent. Bastnaesite, first discovered in 1818 at Bastnaes, Sweden (Glass and Smalley 1945), constitutes an important RE ore and occurs as a high grade accessory mineral of igneous or hydrothermal origin, for example in Mountain Pass (California), Bayan Obo (China) and Wingu Hill (Tanzania) (Head and Holley 1963). The Molycorp operation at Mountain Pass CA (Pradip 1981a) was the largest producer of rare earths until the late 1990s when low cost Chinese production hit the global market and now constitutes 97 % of the world's RE production. Today there is some interest in the U.S. and Canada in renewed RE mining.

Bastnaesite represents a family of RE carbonate minerals [$RE(OH/F)CO_3$] which mostly contain light rare earths (LRE) - La, Ce, Nd and Pr and trace amounts of heavy rare earths (HRE) - Y, Dy, Lu, Eu and others (Fleischer 1978). Its structure consists of RE-F sheets separated by carbonate ions and is related to other RE fluorocarbonate minerals such as parisite [$CaRE_2(CO_3)_2F_2$], roentgenite [$Ca_2RE_3(CO_3)_5F_3$] and synchysite [$CaRE(CO_3)_2F$], where bastnaesite - like sheets are interlayered with sheets of $CaCO_3$ (Vlasov 1964). As the trivalent RE ions have similar crystal chemistry to $Ca^{2+}$, they substitute for Ca in rock forming minerals, and

these RE bearing minerals are active participants in metamorphic reactions on the geologic time scale (Lipin and Mckay 1989). These fluorocarbonates are known to have grown from fluids containing both HF and $CO_2$ and are potential indicators of relative abundances of $CO_2$ and HF (Jones and Wood 1992). Being carbonates, they also can play a role in controlling the global carbon cycle, although they are not major sources or sinks of carbon. While both F and OH bastnaesites are found in nature, the F form is predominant (Jones and Wood 1992). Several reports document bastnaesites from various locations in terms of structure, composition, phase relations and reactivity with other RE accessory minerals (Exley 1980; Smith et al. 1999).

The first efforts to synthesize bastnaesite phases date back to 1950s (George et al. 1959). However it was not until the early 1970s that these phases were studied in terms of structural aspects and compositional variability. In 1973 Haschke proposed phase equilibria in the lanthanum - hydroxide - fluoride - carbonate system as a function of temperature and pressure by synthesizing a series of solid solutions in the $La(OH)_{1-x}F_xCO_3$ system (Haschke 1975; Haschke and Eyring 1971). These investigations provide possible reaction paths for the geochemical formation of bastnaesite. There are recent reports on the crystallization mechanism of OH bastnaesite under hydrothermal conditions (Vallina et al. 2014). In recent years synthetic bastnaesites have gained increased attention as they are used as precursors for synthesis of rare earth oxycarbonates ($RE_2O_2CO_3$) and oxyfluorides (REOF), which are excellent host lattices for phosphors (Lee and Jung 2013; Janka and Schleid 2009). RE hydroxycarbonates are also of interest for optical technologies (Chakhmouradian and Wall 2012). Despite this renewed interest, there are no reliable thermodynamic data available in the literature for bastnaesites. Limited reports on the thermal stability of bastnaesite phases indicate that fluoride phase always persists to higher temperatures than its hydroxide counterpart (Hsu 1992).

This implies that the F – phase could be stable at magmatic conditions while the OH – phase exists only in low temperature environments (Hsu 1992). Based on solubility product and stability constant measurements from solubility and titration experiments, a speciation diagram has been proposed for the $CeFCO_3$ system (Pradip et al. 2013).

In this paper we report the enthalpy of formation for some synthetic bastnaesite phases by direct measurements using high temperature oxide melt solution calorimetry. For this purpose we carried out synthesis and characterization of F – bastnaesites (La and Ce) and both polymorphs of OH – bastnaesites of several RE (La, Ce, Y, Dy and Nd).

## Experimental Methods

*Synthesis*

A summary of the synthesis conditions of both F and OH – bastnaesites is given in Table 1. The detailed procedure used for the syntheses is described below.

*F – bastnaesites*: $REFCO_3$ (RE = La and Ce) phases were synthesized by urea hydrolysis in the presence of $NH_4F$ as a source of $F^-$. In a typical synthesis 0.02 mol of $RE(NO_3)_3$ was dissolved in 20 mL of deionized (DI) water and was added dropwise to a 50 mL of solution containing 0.02 mol of $NH_4F$. The mixture was stirred for 30 min and 0.04 mol of urea was added. The resulting suspension was aged at 90 °C for 20 h and the precipitate obtained was separated by centrifugation, washed with DI water and dried at 60 °C.

*OH – bastnaesites:* $REOHCO_3$ (RE = La, Ce, Y, Nd and Dy) were synthesized by three different aqueous methods, (a) urea hydrolysis and (b) base hydrolysis of $RECl_3$ using sodium carbonate and (c) water hydrolysis of $RE(CO_3)_3$. In a typical synthesis by urea hydrolysis 0.02 mol of $RECl_3$ and 0.01 mol of urea were dissolved in 50 mL of DI water and stirred at room

temperature for 30 min. The solution was then transferred to a Teflon lined autoclave and heated at 180 °C for 3 h. The precipitate was obtained after cooling and subsequently separated by centrifugation, washed with DI water 3 times, and dried at 60 °C. For base hydrolysis a 50 mM solution of $RECl_3$ was added to a 50 mM solution of $Na_2CO_3$ at room temperature, stirred at room temperature for 30 min and transferred to a Teflon-lined autoclave, followed by hydrothermal treatment at 180 °C for 48 h. After cooling the autoclave to room temperature, the precipitate was separated by centrifugation, washed with DI water several times and dried in an oven at 60 °C. For hydrolysis of $RE(CO_3)_3$ in water, 5g of rare earth carbonate was taken in 100 mL water and heated first at 90 °C for 20 h and then at 100 °C for 1 h. The product was separated by centrifugation and dried at 60 °C.

*Characterization*

Powder X-ray diffraction patterns (XRD) of the synthesized samples were recorded using a Bruker AXS D8 Advance diffractometer with CuKa radiation, Kα = 1.5418 Å, to identify the phases. The Rietveld technique was employed for structure refinement of all the samples using X'pert HighScore Plus software. All the structure refinements were carried out using the published structure models. When there was an impurity phase in the sample, phase fractions were obtained by two phase refinements.

Thermogravimetric analysis (TGA) was performed to determine the water content in the samples using a Netzsch 449 thermal analysis system in a dynamic Ar atmosphere (40mL/min, 25 - 800 °C, 5 °C/min, Pt crucible). The data were analyzed using Netzsch Proteus software. The overall RE content in the samples was measured by inductively coupled plasma mass spectrometry (ICP-MS) with an Agilent Technologies 7500a instrument. A known amount of sample was dissolved in ~0.1 mL of ICP grade HCl and diluted with Millipore water. Fourier

transform infrared attenuated total reflectance spectra (ATR - FTIR) of all the samples were recorded using a Bruker Model Alpha-P IR spectrometer (diamond ATR cell, 4 $cm^{-1}$ resolution, 400 - 4000 $cm^{-1}$).

*High temperature oxide melt solution calorimetry*

High temperature oxide melt solution calorimetry was performed using a custom built isoperibol Tian-Calvet microcalorimeter as described by Navrotsky (1977; 1997). Molten sodium molybdate was used as a solvent at 700 °C. The calorimeter was calibrated using the heat content of high purity $\alpha$-$Al_2O_3$. Oxygen was flushed through the glassware at 60 mL/min to maintain constant atmosphere and bubbled through the solvent at 30 mL/min using a bubbling tube to remove evolved gases, aid dissolution, and prevent local saturation of the solvent. In a typical experiment ~5 mg of loosely pelletized sample was dropped into the solvent. The measured heat effect (heat of drop solution, $\Delta H_{ds}$), includes the heat content of the sample, the heat effect associated with desorbing and vaporizing water, decarbonation and the heat of dissolution of the oxide component of the sample in the high temperature solvent. Heats of drop solution of the binary oxides were taken from previously published work (Navrotsky 2014).

## Results and Discussion

Two F – bastnaesites (La and Ce) were successfully synthesized by urea hydrolysis in the presence of $NH_4F$. Among the OH – bastnaesites, two phase pure samples with hexagonal structure (La and Nd) were synthesized. Four OH – bastnaesite samples with orthorhombic structure were prepared (La, Ce, Dy and Y), among which the one containing Dy was phase pure and the others contained oxide impurities. A summary of samples used for calorimetric measurements is given in Table 1

Rietveld fits of the PXRD patterns of the two F – bastnaesites are shown in Figure S1 in the supplementary information. Both $LaFCO_3$ and $CeFCO_3$ crystallize in hexagonal crystal structure. PXRD pattern of $LaFCO_3$ could be refined using published crystal structure (ICSD no: 26678) with $a$ = 7.180 (8) Å and $c$ = 4.912 (6) Å. PXRD pattern of $CeFCO_3$ was refined using a published crystal structure (ICSD no: 27591) with a = 7.201 (1) Å and c = 9.970 (2) Å. The results of refinements of both F – bastnaesites are listed in Table 2. In the crystal structure of $LaFCO_3$, fluoride anions are present in two crystallographically distinct sites. $La^{3+}$ cations form hexagonal layers with both the fluoride ions. Oxygen atoms of the carbonate are present in two different sites as well, resulting in two topologically different carbonate anions sandwiched between the hexagonal layers formed by $La^{3+}$ and $F^-$. $CeFCO_3$ exhibits a similar structure, but with an elongated $c$ - parameter corresponding to two hexagonal layers formed by Ce and F ions, unlike in $LaFCO_3$ where there is one layer per unit cell. A view of crystal structure along the $c$ - direction showing the hexagonal layers formed by Ce and F ions is shown in Figure 1a, which is isostructural with $LaFCO_3$. The structure along the $b$-direction, showing carbonate in two different orientations between these hexagonal layers, is shown in Figure 1b. The $Ce^{3+}$ cation is in irregular coordination with eight O and three in - plane F ions, resulting in an overall coordination number of 11 for RE in a distorted tricapped trigonal prismatic arrangement.

OH – bastnaesite, on the other hand, is known to exist in two different polymorphic modifications - hexagonal and orthorhombic (Sum 1986). Our attempts to synthesize both polymorphs in the Y, La, Ce, Nd and Dy were partially successful. While most of our synthetic efforts produced a mixture of the two polymorphs, we found one methodology to successfully synthesize single phase precipitates for each of the $REOHCO_3$ systems, see Table 1. Both hexagonal and orthorhombic polymorphs were obtained for $LaOHCO_3$ and the Rietveld fit of the

PXRD patterns are shown in Figure S2. The hexagonal polymorph was phase pure and the orthorhombic polymorph had $La_2O_3$ impurities. Two phase refinement was performed for the orthorhombic polymorph to quantify the amount of impurity, which was found to be 6.5 %. The obtained refined lattice parameters and goodness of fit parameters are listed in Table 2. The two polymorphs of OH – bastnaesites are not isostructural with F – bastnaesite, although the metal sub-lattice looks similar for the hexagonal polymorph. The crystal structures of both polymorphs are shown in Figure 2. In both cases each La is coordinated with 11 O atoms. Distortion in carbonate polyhedra is observed, probably due to the hydrogen bonding with $OH^-$ ions. Further the OH anions are not coplanar with the La cations, unlike those in $LaFCO_3$.

PXRD patterns of $CeOHCO_3$ (orthorhombic), $YOHCO_3$ (orthorhombic), $NdOHCO_3$ (hexagonal) and $DyOHCO_3$ (orthorhombic) are shown in Figure S3. $CeOHCO_3$ and $YOHCO_3$ contained $RE_2O_3$ impurities, quantified to be 5.9 and 6.3 wt % respectively. $NdOHCO_3$ and $DyOHCO_3$ were phase pure. The refined lattice parameters of all the OH - bastnaesites are listed in Table 2.

Thermogravimetric (TG) curves of the two F – bastnaesites and that of OH bastnaesites are shown in Figure S4. A total mass loss of 20 % and 22 % was observed up to 550 °C for $LaFCO_3$ and $CeFCO_3$ respectively, which corresponds to decarbonation, leading to residual metal oxyfluorides. OH – bastnaesites showed no significant mass loss below 150 °C. A single step mass loss was observed for $CeOHCO_3$ and $DyOHCO_3$, indicating that decarbonation and dehydroxylation occur simultaneously. In contrast, the other OH – bastnaesites showed two-step mass losses, suggesting that decarbonation and dehydroxylation occur at different temperatures.

Attenuated total reflectance (ATR) spectra of F and OH – bastnaesites are shown in Figure S5. Both the F – bastnaesites exhibit peaks corresponding to carbonate vibrations at 1440 and 865 $cm^{-1}$, whereas all the OH – bastnaesites exhibit multiple absorption bands in the same frequency range due to lowering of local symmetry of carbonate. This could be due to distortion of the carbonate ion by the polarizing influence of the OH group. Two different kinds of distorted carbonate groups were also seen in these OH – bastnaesites. The observed peaks could be attributed to $\nu_1$ (1070 - 1100 $cm^{-1}$), $\nu_2$ (850 - 880 $cm^{-1}$), $\nu_3$ (1400 - 1510 $cm^{-1}$) and $\nu_4$ (690 - 730 $cm^{-1}$) modes of carbonate. In addition, two weak but discernable sharp peaks were observed between 3600 and 3400 $cm^{-1}$ due to OH vibrations. The infrared spectrum of the orthorhombic polymorphs is less complicated than that of the hexagonal polymorph.

*High temperature oxide melt solution calorimetry*

Enthalpies of drop solution of all the samples and the constituents used in thermodynamic cycle are listed in Table 3. Enthalpies of formation of F – bastnaesites were calculated from a mixture of constituent oxides and fluorides and the thermochemical cycle used for the calculation is shown in Table 4. Since oxygen was bubbled through and over the solvent during the experiments, the dissolved state of cerium is $Ce^{4+}$. The calculated enthalpy of formation of $LaFCO_3$ and $CeFCO_3$ were -173.07 ± 2.40 and -141.24 ± 2.58 kJ/mol, respectively. The strongly exothermic values indicate that these F bastnaesites are significantly stable compared to mechanical mixture of their oxide and fluoride components and $CO_2$ gas.

Thermodynamic cycles used for the calculation of formation enthalpies of OH – bastnaesites from their constituent oxides are shown in Table 5. Enthalpy of formation of the two hexagonal polymorphs $LaOHCO_3$ and $NdOHCO_3$ are -196.55 ± 1.64 and -165.01 ± 3.05 kJ/mol, respectively.

Enthalpies of formation of the four orthorhombic polymorphs are -227.38 ± 2.87, -166.03 ± 3.35, -133.72 ± 1.90 and -105.60 ± 3.82 kJ/mol for La, Ce, Dy and Y OH – bastnaesites, respectively. A plot of $RE^{3+}$ cation radius (Shannon and Prewitt 1969) vs. enthalpy of formation is shown in Figure 3.

## Discussion

As seen from Figure 3, the formation enthalpies of the bastnaesite phases from $RE_2O_3$, $CO_2$, and $H_2O$ or HF become increasingly negative with increase in ionic radius of the $RE^{3+}$ cation. A similar general trend has been observed among several other ternary compounds of rare earths for a given structure, including phosphates, perovskites, aluminates and silicates (Navrotsky 2001 and Ushakov et al. 2001).

Among RE mineral phases, bastnaesite is the lowest temperature RE mineral and is stable within the garnet zone (Savko and Bazikov 2011). One of the hypotheses is that the bastnaesites could have been formed during metamorphism (Savko and Bazikov 2011). Quite similar to monazite, bastnaesites show light rare earth (LRE) selectivity and have a coordination number of 11 for RE cations. As temperature increases, bastnaesite is known to react with apatite to form monazite (Savko and Bazikov 2011 and Smith et al 1999), as represented by reaction (1).

$$\text{Bastnaesite} + \text{Apatite} \rightarrow \text{Monazite} + Ca^{2+}\ (\text{in silicates}) + \text{fluid}\ (HF, CO_2, H_2O) \quad (1)$$

To consider this reaction for different bastnaesites, we compare the enthalpy of formation of bastnaesites and RE phosphates. The trends in variation of formation enthalpy of monazite and bastnaesite for different RE are similar, see Figure 4a, where with increasing ionic radius of $RE^{3+}$, the formation enthalpy becomes more negative (this work and Ushakov et al. 2001). While the observed trends are similar, it is obvious that formation enthalpies from binary oxides are

more negative for phosphates than for bastnaesites. Furthermore the difference in formation enthalpies of monazite and bastnaesite ($\Delta Hf_{diff} = \Delta Hf_{monazite} - \Delta Hf_{bastnaesite}$) for different RE gives an indication of the variation of enthalpy and free energy with RE for reaction (1), assuming the apatite, Ca-silicate, and fluid phases remain similar. A plot of difference in formation enthalpies of RE monazite and RE bastnaesite is shown in Figure 4b. The difference is least negative for both the F – bastnaesites, $LaFCO_3$ and $CeFCO_3$. The difference is comparatively more negative for OH – bastnaesites, with La being least and Y being most negative. The difference thus seems to become less negative with increasing radius of $RE^{3+}$, consistent with the LRE preference of bastnaesite. The least negative difference, observed for F – bastnaesite, both in case of La and Ce, supports the observation that natural bastnaesites are strongly Ce and La - selective. Ce is the element which is most abundant in natural bastnaesites and La is the second. In some monazite deposits, the presence of F also indicates that monazite was formed at the expense of bastnaesite and apatite (Savko and Bazikov 2011; Smith et al 1999) which is also supported by their energetic stabilities.

In nature F – bastnaesite is dominant and OH – bastnaesite is rare. OH – bastnaesites are known to occur only in low temperature zones which are essentially devoid of F. The stability relations at $P_F$ = 1 kbar and T = 400 - 900 °C in a part of (Ce, La)-F-H-C-O system indicate that the F – bastnaesites of both La and Ce have stability fields wider than their OH – counterparts by 50 °C and 120 °C respectively (Hsu 1992). This finding is also supported by Haschke (1975). From the only two synthetic analogues available for comparison, it can be seen from Table 3 that the enthalpy of formation calculated from binary oxides of the OH – bastnaesites of both La and Ce are more negative than those of their F – counterparts calculated from a mixture of binary oxide and fluoride end members. These values do not help for direct comparison, since they were

calculated from different end members. We thus compare the enthalpy of formation values calculated from elements for these phases as shown in Table 4 and 5. The enthalpies of formation calculated from elements indicate that the F – bastnaesites are more stable than their OH – counterparts (last column of Table 3). Also, the enthalpy of reaction calculated for the conversion of $RECO_3F$ to $RECO_3OH$, which corresponds to substitution of $F^-$ by $OH^-$, is positive (Eq. 2 ) for both La and Ce (100.59 and 69.76 kJ/mol for La containing hexagonal and orthorhombic OH - polymorphs respectively and 106.49 kJ/mol for Ce). These positive values strongly suggest that the reaction is not spontaneous, since entropy effects are expected to be relatively small.

$$RECO_3F + H_2O\ (l) \rightarrow RECO_3OH + HF\ (aq) \qquad (2)$$

Thus the F – bastnaesites are thermodynamically more stable than their OH – analogues. This observation explains why F – bastnaesite is more common in the Earth's crust than OH – bastnaesite and also explains the ease of formation of the former in laboratory conditions even under low F content in the aqueous phase.

## Implications

While in reality bastnaesite is a complex solid solution with different RE and in some cases with both $OH^-$ and $F^-$, in this paper we have reported the thermodynamic properties of $F^-$ and $OH^-$ end members. The new data should be useful for modelling the formation of the mineral and leaching and processing of the ore. The calorimetric data confirm the increasing stability of bastnaesites with light rare earths and the greater stability and persistence to higher temperature of the fluoride end members compared to the hydroxides, thus providing a thermodynamic

justification for the pattern of bastnaesite occurrences in nature. The data provide a starting point for the modelling of complex bastnaesite solid solutions.

## Acknowledgments

The first steps of this study, including synthesis and characterization, were supported by the National Science Foundation, Division of Earth Sciences with contributions from the NSF - wide SUSChem initiative (grant EAR - 1321410). The latter part of the study, including calorimetry, data analysis, and manuscript preparation, was supported by the Critical Materials Institute, an Energy Innovation Hub funded by the U.S. Department of Energy, Office of Energy Efficiency and Renewable Energy, Advanced Manufacturing Office.

## References

Alonso, E., Sherman, A.M., Wallington T.J., Everson M.P., Field F.,R, Roth R., Kirchain, R E. (2012) Evaluating rare earth element availability: a case with revolutionary demand from clean technologies. Environmental Science and Technology, 46, 3406–341

Chakhmouradian, A.R., Wall, F. (2012) Rare earth elements: minerals, mines, magnets. Elements, 8, 333-340

Donnay, G., and Donnay, J.D.H. (1953) The crystallography of bastnaesite, parisite, roentgenite, and synchisite. American Mineralogist, 38, 932-938

Exley, R. A. (1980) Microprobe studies of REE-rich accessory minerals: Implications for Skye granite petrogenesis and REE mobility in hydrothermal systems. Earth and Planetary Science Letters, **1980**, 48, 97-110

Fleischer, M. (1978) Relative proportions of the lanthanides in minerals of the bastnaesite group. Canadian Mineralogist, 16, 361-363

Glass, J. J., Smalley, R. G. (1945) Bastnaesite. American Mineralogist, 30, 601-615

Gschneidner, K. A. (1981) Industrial Applications of Rare Earth Elements, ACS Symposium Series, 164, 1-297

Haschke, J. M. (1975) The lanthanum hydroxide fluoride carbonate system: The preparation of synthetic bastnaesite. Journal of Solid State Chemistry, 12, 115-121

Haschke, J. M., Eyring, L. (1971) Hydrothermal equilibriums and crystal growth of rare earth oxides, hydroxides, hydroxynitrates, and hydroxycarbonates. Inorganic Chemistry, 10, 2267-2274

Head, E.L., Holley, C.E. (1963) Rare-earth carbonate, Rare Earth Research Proceedings of Third Conference, Gordon and Breach, 51-63

Hsu, L. C. (1992) Synthesis and stability of bastnaesites in a part of the system (Ce,La)-F-H-C-O. Mineralogy and Petrology, 47, 87-101

Humphries, M. (2010) Rare Earth Elements: The Global Supply Chain: Congressional Research Service; The Library of Congress: Washington, DC, USA.

Janka, O., Schleid, T. (2009) Facile Synthesis of Bastnaesite-Type LaF[$CO_3$] and Its Thermal Decomposition to LaOF for Bulk and $Eu^{3+}$-Doped Samples. European Journal of Inorganic Chemistry, 3, 357-362.

Jansen, G. J., Magin, G. B., Levin. B. Synthesis of bastnaesite (1959) American Mineralogist, 44, 180-190

Vlasov, K. A. (1964) Geochemistry, mineralogy and genetic types of deposits of rare elements. Mineralogy of Rare Elements, 2, 264

Keith, R. L. (2011) Principal Rare Earth Elements Deposits of the U. S.: A Summary of Domestic Deposits and a Global Perspective, 1-96

Kirillov, A.S. (1964) Hydroxyl-bastnasite, a new mineral variety. Zapiski Vsesoyuznogo Mineralogicheskogo Obshchestva, 159, 93-95

Lee, M.H., Jung, W.S. (2013) Hydrothermal Synthesis of LaCO3OH and $Ln^{3+}$-doped $LaCO_3OH$ Powders under Ambient Pressure and Their Transformation to $La_2O_2CO_3$ and $La_2O_3$. Bulletin of the Korean Chemical Society, 34, 3609-3614

Lipin, B.R., Mckay, G.A. (1989) Geochemistry and mineralogy of rare earth elements. Mineralogical Society of America, 21, 259-302

Maksimovic, Z., Panto, G. (1985) Hydroxyl-bastnaesite-(Nd), a new mineral from Montenegro, Yugoslavia. Mineralogical Magazine, 49, 717-720

McLellan, B.C., Corder, G.D., Ali, S.H. (2013) Sustainability of Rare Earths – An Overview of

the State of Knowledge. Minerals, 3, 304–317

Navrotsky, A. (1977) Progress and new directions in high temperature calorimetry. Physics and Chemistry of Minerals, 2, 89–104

Navrotsky, A. (2001) Systematic trends and prediction of enthalpies of formation of refractory lanthanide and actinide ternary oxide phases. Ceramic Transactions, 137-145

Navrotsky, A. (1997) Progress and new directions in high temperature calorimetry: revisited. Physics and Chemistry of Minerals, 24, 222–241

Navrotsky, A. (2014) Progress and new directions in calorimetry: a 2014 perspective. Journal of American Ceramic Society. 97, 3349-3359

Pathak, A. K., Khan, M. Gschneider, K. A., McCallum, R.W., Zhou, L., Sun, K., Dennis, K.W., Zhou, C., Pinkerton, F. E., Kramer, M. J., Pecharsky, V. K. (2015) Cerium: an unlikely replacement of dysprosium in high performance Nd–Fe–B permanent magnets. Advanced Materials, 27, 2663–2667

Pradip (1981) The surface properties and flotation of rare earth minerals, Ph.D. Thesis, University of California, Berkeley.

Pradip., Li, H. C.C., Fuestenau, D. W. (2013) The Synthesis and Characterization of Rare Earth Fluocarbonates. KONA Powder and Particle Journal, 30, 193-200

Savko, K. A., Bazikov, N. S. (2011) Phase equilibria of bastnaesite, allanite, and monazite: bastnaesite-out isograde in metapelites of the Vorontsovskaya group, Voronezh crystalline massif. Petrology, 19, 445-469

Shannon, R. D., Prewitt, C. T. (1969) Effective ionic radii in oxides and fluorides. Acta Crystallographica. B25, 927-946

Smith, M.P., Henderson, P., and Peishan, Z., (1999) Reaction Relationships in the Bayan Obo Fe-REE-Nb Deposit, Inner Mongolia, China: Implications for the Relative Stability of Rare Earth Element Phosphates and Fluorocarbonates, Contributions to Mineralogy and Petrology, 134, 294–310.

Sun, J., Kyotani, T., Tomita, A., (1986) Preparation and characterization of lanthanum carbonate hydroxide, Journal of Solid State Chemistry, 64, 94-99

Ushakov, S.V., Helean, K.B., Navrotsky, A., and Boatner, L.A., (2001) Thermochemistry of Rare-Earth Orthophosphates, Journal of Materials Research, 16, 2623–2633

Vallina, B., Blanco, J. D.R, Blanco, J. A., Benning, L. G.,(2014) The effect of heating on the morphology of crystalline neodymium hydroxycarbonate, $NdCO_3OH$, Mineralogical Magazine, 78, 1391-1397

Williams-Jones, A. E. Wood, S. A., (1992) A preliminary petrogenetic grid for REE fluorocarbonates and associated minerals, Geochimica et Cosmochimica Acta, 56, 725-738

## Figure Captions

Figure 1. Crystal structure of $CeFCO_3$ shown along (a) c-axis and along (b) b- axis

Figure 2. Structures of orthorhombic (left panel) and hexagonal (right panel) polymorphs of $LaOHCO_3$.

Figure 3. Enthalpy of formation of F/OH-bastnaesite as a function of ionic radii of $RE^{3+}$ cation

Figure 4. Comparison of enthalpy of formation of bastnaesite with $REPO_4$. In the inset is a plot of difference in enthalpy of formation of bastnaesite and monazite for different REs.

**Table 1.** Bastnaesite samples used for calorimetric studies, their synthesis conditions and crystal systems

| Sample | Method of synthesis/Temperature | Crystal system | % oxide impurities |
|---|---|---|---|
| $LaFCO_3$ | Urea hydrolysis /90 °C | Hexagonal | - |
| $CeFCO_3$ | Urea hydrolysis/ 90 °C | Hexagonal | - |
| $LaOHCO_3$-Hex | Hydrolysis of $La_2(CO_3)_3$/ 90 °C | Hexagonal | - |
| $LaOHCO_3$-ortho | Urea hydrolysis/ 180 °C | Orthorhombic | 6.1 |
| $CeOHCO_3$ | Urea hydrolysis/ 180 °C | Orthorhombic | 5.9 |
| $DyOHCO_3$ | Hydrolysis of REE nitrate with $Na_2CO_3$/220 °C | Orthorhombic | - |
| $YOHCO_3$ | Urea hydrolysis/ 180 °C | Orthorhombic | 6.3 |
| $NdOHCO_3$ | Hydrolysis of REE nitrate with $Na_2CO_3$/220 °C | Hexagonal | - |

**Table 2**. Summary of results of Rietveld refinements of F and OH - bastnaesites

| Bastnaesite | Space group | Cell parameters/Å |
|---|---|---|
| $LaFCO_3$ | P-6 2m | *a* = 7.180 (8)<br>*c* = 4.912 (6) |
| $CeFCO_3$ | P-6 2c | *a* = 7.201 (1)<br>*c* = 9.970 (2) |
| $LaOHCO_3$ | P-6 | *a* = 12.647 (2)<br>*c* = 10.025 (4) |
| $LaOHCO_3$ | Pnma | *a* = 7.270 (1), b = 5.022 (8)<br>c = 8.590 (1) |
| $CeOHCO_3$ | P212121 | *a* = 5.005 (4), *b* = 8.535 (7),<br>*c* = 7.305 (6) |
| $YOHCO_3$ | P212121 | *a* = 4.809 (1), *b* = 6.957 (3),<br>*c* = 8.466 (5) |
| $DyOHCO_3$ | P212121 | *a* = 4.834 (3), *b* = 6.980 (1),<br>*c* = 8.444 (2) |
| $NdOHCO_3$ | P-6 | *a* = 12.327 (1)<br>*c* = 9.880 (4) |

**Table 3.** Thermochemical data for F and OH - bastnaesites and for the constituents used for enthalpy of formation calculation

| Sample | Enthalpy of drop solution (kJ/mol) | Enthalpy of formation from oxides at 298 K (kJ/mol) | Enthalpy of formation from elements (kJ/mol) |
|---|---|---|---|
| $LaF_3$ | 95.87 ± 2.9 | | -1732.1 ± 1.2 |
| $La_2O_3$ | -225.1 ± 3.16 | | -1791.6 ± 1.0 |
| $CeF_3$ | 89.58 ± 2.3 | | -1726.1 ± 1.6 |
| $Ce_2O_3$ | | 371.6 ± 5.0 | -1799.8 ± 1.8 |
| $CeO_2$ | 74.37 ± 0.75 | | -1090.4 ± 0.8 |
| $Y_2O_3$ | -120.74 ± 0.94 | | -1932.8 ± 5.2 |
| $Nd_2O_3$ | -163.36 ± 3.44 | | -1806.8 ± 3.0 |
| $Dy_2O_3$ | -114.88 ± 2.2 | | -1863.4 ± 5.0 |
| $LaFCO_3$ | 162.50 ± 1.95 | -173.07 ± 2.4 | -1729.37 ± 2.72 |
| $CeFCO_3$ | 126.27 ± 1.77 | -141.24 ± 2.58 | -1708.85 ± 4.09 |
| $LaOHCO_3$-hex | 150.57 ± 0.45 | -196.55 ± 1.64 | -1628.78 ± 2.53 |
| $LaOHCO_3$-ortho | 181.40 ± 2.4 | -227.38 ± 2.87 | -1659.61 ± 4.48 |
| $CeOHCO_3$ | 115.74 ± 2.10 | -166.03 ± 3.35 | -1602.36 ± 3.65 |
| $DyOHCO_3$ | 142.85 ± 1.55 | -133.72 ± 1.90 | -1601.85 ± 5.15 |
| $NdOHCO_3$ | 149.90 ± 2.52 | -165.01 ± 3.05 | -1604.89 ± 5.74 |
| $YOHCO_3$ | 111.80 ± 4.8 | -105.6 ± 4.82 | -1608.49 ± 6.87 |

**Table 4**. Thermochemical cycle used for the calculation of enthalpy of formation of F-bastnaesites

| **LaFCO$_3$** | |
|---|---|
| (1) $LaCO_3F_{(s,\ 25\ °C)} \rightarrow 0.33\ La_2O_3{}_{(sol,\ 700\ °C)} + 0.33LaF_{3\ (sol,\ 700\ °C)} + CO_{2\ (g,\ 700\ °C)}$ | $\Delta H_1$ |
| (2) $La_2O_{3\ (s,\ 25\ °C)} \rightarrow La_2O_{3\ (sol,\ 700\ °C)}$ | $\Delta H_2$ |
| (3) $LaF_{3\ (S,\ 25\ °C)} \rightarrow LaF_{3\ (sol,\ 700\ °C)}$ | $\Delta H_3$ |
| (4) $CO_{2\ (g,\ 25\ °C)} \rightarrow CO_{2\ (g,\ 700\ °C)}$* | $\Delta H_4$ |
| (5) $2La_{(s,\ 25°C)} + 3/2O_{2\ (g,\ 25\ °C)} \rightarrow La_2O_3{}_{((S,\ 25\ °C)}$ | $\Delta H_5$ |
| (6) $La_{(s,\ 25°C)} + 3/2F_{2(g,\ 25°C)} \rightarrow LaF_{3(s,\ 25°C)}$ | $\Delta H_6$ |
| (7) $C_{(s,\ 25°C)} + O_{2\ (g,\ 25°C)} \rightarrow CO_{2\ (g,\ 25°C)}$ | $\Delta H_7$ |
| (8) $0.33\ La_2O_{3\ (s,\ 25\ °C)} + 0.33LaF_{3\ (S,\ 25\ °C)} + CO_{2(g,\ 25\ °C)} \rightarrow LaCO_3F_{(s,\ 25\ °C)}$ | $\Delta H_{f,ox}$ |
| (9) $La_{(s,\ 25°C)} + 1/2F_{2(g,\ 25°C)} + C_{(s,\ 25°C)} + 3/2\ O_{2\ (g,\ 25°C)} \rightarrow LaCO_3F_{(s,\ 25\ °C)}$ | $\Delta H_{f,el}$ |
| $\mathbf{\Delta H_{f,ox} = -\Delta H_1 + 0.33\Delta H_2 + 0.33\Delta H_3 + \Delta H_4}$ | |
| $\mathbf{\Delta H_{f,el} = \Delta H_{f,ox} + 0.33\Delta H_5 + 0.33\Delta H_6 + \Delta H_7}$ | |
| **CeFCO$_3$** | |
| (1) $CeCO_3F_{(s,\ 25\ °C)} + 0.165O_{2(g,\ 700C)} \rightarrow 0.667\ CeO_{2\ (sol,\ 700\ °C)} + 0.33CeF_{3(sol,\ 700\ °C)} + CO_{2\ (g,\ 700\ °C)}$ | $\Delta H_1$ |
| (2) $CeO_{2\ (s,\ 25\ °C)} \rightarrow CeO_{2\ (sol,\ 700\ °C)}$ | $\Delta H_2$ |
| (3) $CeF_{3\ (S,\ 25\ °C)} \rightarrow CeF_{3\ (sol,\ 700\ °C)}$ | $\Delta H_3$ |
| (4) $CO_{2\ (g,\ 25\ °C)} \rightarrow CO_{2\ (g,\ 700\ °C)}$* | $\Delta H_4$ |
| (5) $O_{2\ (g,\ 25C)} \rightarrow O_{2\ (g,\ 700\ °C)}$ | $\Delta H_5$ |
| (6) $Ce_2O_{3\ (s,\ 25\ °C)} + 0.5O_{2\ (g,\ 25\ C)} \rightarrow 2CeO_{2\ (s,\ 25\ °C)}$ | $\Delta H_6$ |
| (7) $2Ce_{(s,\ 25\ °C)} + 3/2\ O_{2\ (g,\ 25\ °C)} \rightarrow Ce_2O_{3\ (s,\ 25\ °C)}$ | $\Delta H_7$ |
| (8) $Ce_{(s,\ 25\ °C)} + 3/2\ F_{2\ (g,\ 25\ °C)} \rightarrow CeF_{3\ (S,\ 25\ °C)}$ | $\Delta H_8$ |
| (9) $C_{(s,\ 25°C)} + O_{2\ (g,\ 25°C)} \rightarrow CO_{2\ (g,\ 25°C)}$ | $\Delta H_7$ |
| (10) $0.33\ Ce_2O_{3\ (s,\ 25\ °C)} + 0.33CeF_{3\ (S,\ 25\ °C)} + CO_{2(g,\ 25\ °C)} \rightarrow CeCO_3F_{(s,\ 25\ °C)}$ | $\Delta H_{f,ox}$ |
| (11) $Ce_{(s,\ 25°C)} + 1/2F_{2\ (g,\ 25°C)} + C + 3/2\ O_{2(g,\ 25°C)} \rightarrow CeCO_3F_{(s,\ 25°C)}$ | |
| $\mathbf{\Delta H_{f,ox} = -\Delta H_1 + 0.667\Delta H_2 + 0.33\Delta H_3 + \Delta H_4 - 0.165\Delta H_5 + 0.33\Delta H_6}$ | |
| $\mathbf{\Delta H_{f,el} = \Delta H_{f,ox} + 0.33\Delta H_7 + 0.33\Delta H_8 + \Delta H_9}$ | |

* $CO_2$ = 32.07 kJ/mol and $O_2$ = 21.74 kJ/mol (Calculated from heat capacity measurements).

**Table 5**. Thermochemical cycle used to calculate enthalpies of formation of OH-bastnaesites.

| **$RECO_3OH$ (RE – La, Y, Nd and Dy)** | |
|---|---|
| (1) $RECO_3OH_{(s,\ 25\ °C)} \rightarrow 0.5\ RE_2O_{3(sol,\ 700\ °C)} + CO_{2(g,\ 700\ °C)} + 0.5\ H_2O_{(g,\ 700\ °C)}$ | $\Delta H_1$ |
| (2) $RE_2O_{3\ (s,\ 25\ °C)} \rightarrow RE_2O_{3\ (sol,\ 700°\ C)}$ | $\Delta H_2$ |
| (3) $H_2O_{(l,\ 25\ °C)} \rightarrow H_2O_{(g,\ 700\ °C)}$ | $\Delta H_3$ |
| (4) $CO_{2\ (g,\ 25\ °C)} \rightarrow CO_{2\ (g,\ 700°C)}$ | $\Delta H_4$ |
| (5) $2RE_{(s,\ 25\ °C)} + 3/2\ O_{2\ (g,\ 25\ °C)} \rightarrow Ce_2O_{3\ (s,\ 25\ °C)}$ | $\Delta H_5$ |
| (6) $C_{(s,\ 25°C)} + O_{2\ (g,\ 25°C)} \rightarrow CO_{2\ (g,\ 25°C)}$ | $\Delta H_6$ |
| (7) $H_2 + ½\ O_{2\ (g,\ 25°C)} \rightarrow H_2O_{(l,\ 25\ °C)}$ | $\Delta H_7$ |
| (8) $0.5\ RE_2O_{3\ (s,\ 25\ °C)} + CO_{2(g,\ 25\ °C)} + 0.5\ H_2O_{(l,\ 25°C)} \rightarrow RECO_3OH_{(s,\ 25\ °C)}$ | $\Delta H_{f,ox}$ |
| (9) $RE_{(s,\ 25\ °C)} + C_{(s,\ 25\ °C)} + 1/2H_{2(g,\ 25\ °C)} + 2O_{2(g,\ 25\ °C)} \rightarrow RECO_3OH_{(s,\ 25\ °C)}$ | $\Delta H_{f,el}$ |
| $\mathbf{\Delta H_{f,ox} = -\Delta H_1 + 0.5\Delta H_2 + 0.5\ \Delta H_3 + \Delta H_4}$ | |
| $\mathbf{\Delta H_{f,el} = \Delta H_{f,ox} + 0.5\Delta H_5 + 0.5\ \Delta H_7 + \Delta H_6}$ | |
| **$CeCO_3OH$** | |
| (1) $CeCO_3OH_{(s,\ 25\ °C)} + 0.25O_{2(g,\ 700C)} \rightarrow CeO_{2\ (sol,\ 700\ °C)} + CO_{2\ (g,\ 700\ °C)} + 0.5\ H_2O_{(g,\ 700\ °C)}$ | $\Delta H_1$ |
| (2) $CeO_{2\ (s,\ 25\ °C)} \rightarrow CeO_{2\ (sol,\ 700\ °C)}$ | $\Delta H_2$ |
| (3) $CO_{2\ (g,\ 25\ °C)} \rightarrow CO_{2\ (g,\ 700\ °C)}$ | $\Delta H_3$ |
| (4) $O_{2(g,\ 25C)} \rightarrow O_{2(g,\ 700\ °C)}$ | $\Delta H_4$ |
| (5) $Ce_2O_{3\ (s,\ 25\ °C)} + 0.5O_{2\ (g,\ 25\ C)} \rightarrow 2CeO_{2\ (s,\ 25\ °C)}$ | $\Delta H_5$ |
| (6) $H_2O_{(l,25\ °C)} \rightarrow H_2O_{(g,\ 700\ °C)}$ | $\Delta H_6$ |
| (7) $2Ce_{(s,\ 25\ °C)} + 3/2\ O_{2\ (g,\ 25\ °C)} \rightarrow Ce_2O_{3\ (s,\ 25\ °C)}$ | $\Delta H_7$ |
| (8) $C_{(s,\ 25°C)} + O_{2\ (g,\ 25°C)} \rightarrow CO_{2\ (g,\ 25°C)}$ | $\Delta H_8$ |
| (9) $H_2 + ½\ O_{2\ (g,\ 25°C)} \rightarrow H_2O_{(l,\ 25\ °C)}$ | $\Delta H_9$ |
| (10) $0.5Ce_2O_{3\ (s,\ 25\ °C)} + CO_{2(g,\ 25\ °C)} + 0.5\ H_2O_{(l,25\ °C)} \rightarrow CeCO_3OH_{(s,\ 25\ °C)}$ | $\Delta H_{f,ox}$ |
| $\mathbf{\Delta H_{f,ox} = -\Delta H_1 + \Delta H_2 + \Delta H_3 - 0.25\Delta H_4 + 0.5\Delta H_5 + 0.5\ \Delta H_6}$ | |
| $\mathbf{\Delta H_{f,el} = \Delta H_{f,ox} + 0.5\Delta H_7 + 0.5\ \Delta H_9 + \Delta H_8}$ | |

# $\Delta H_{f,el}$ for $CO_2$ and $H_2O$ is -393.51±1.3 and -285.83±0.42 kJ/mol respectively (From Robie and Hemingway 1995)

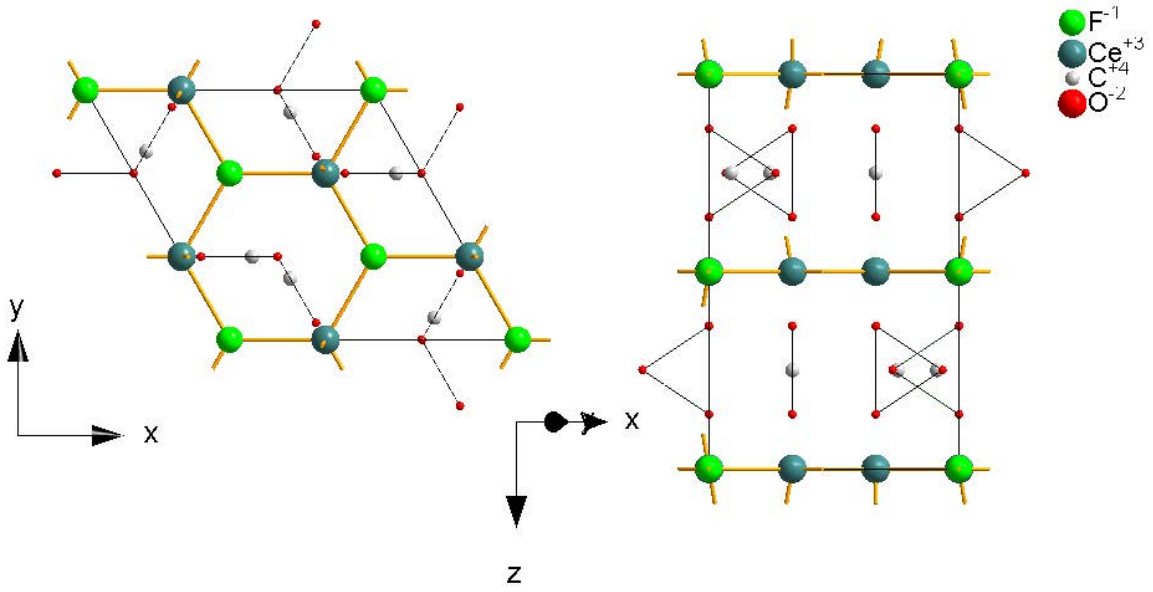


**Figure 1.** Crystal structure of $CeFCO_3$ shown along (a) c-axis and along (b) b- axis

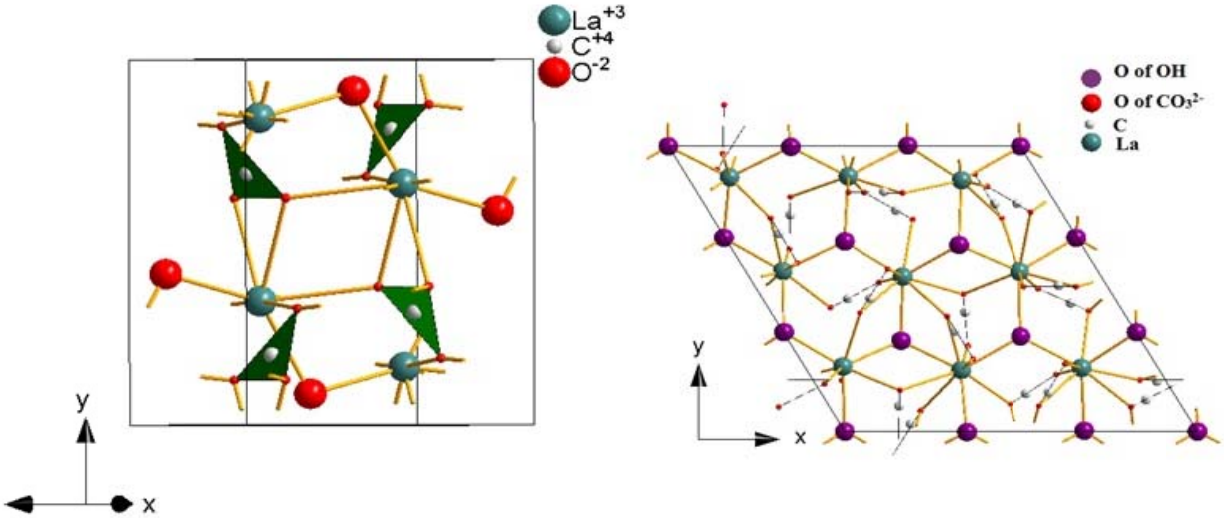


**Figure 2.** Structures of orthorhombic (left panel) and hexagonal (right panel) polymorphs of $LaOHCO_3$.

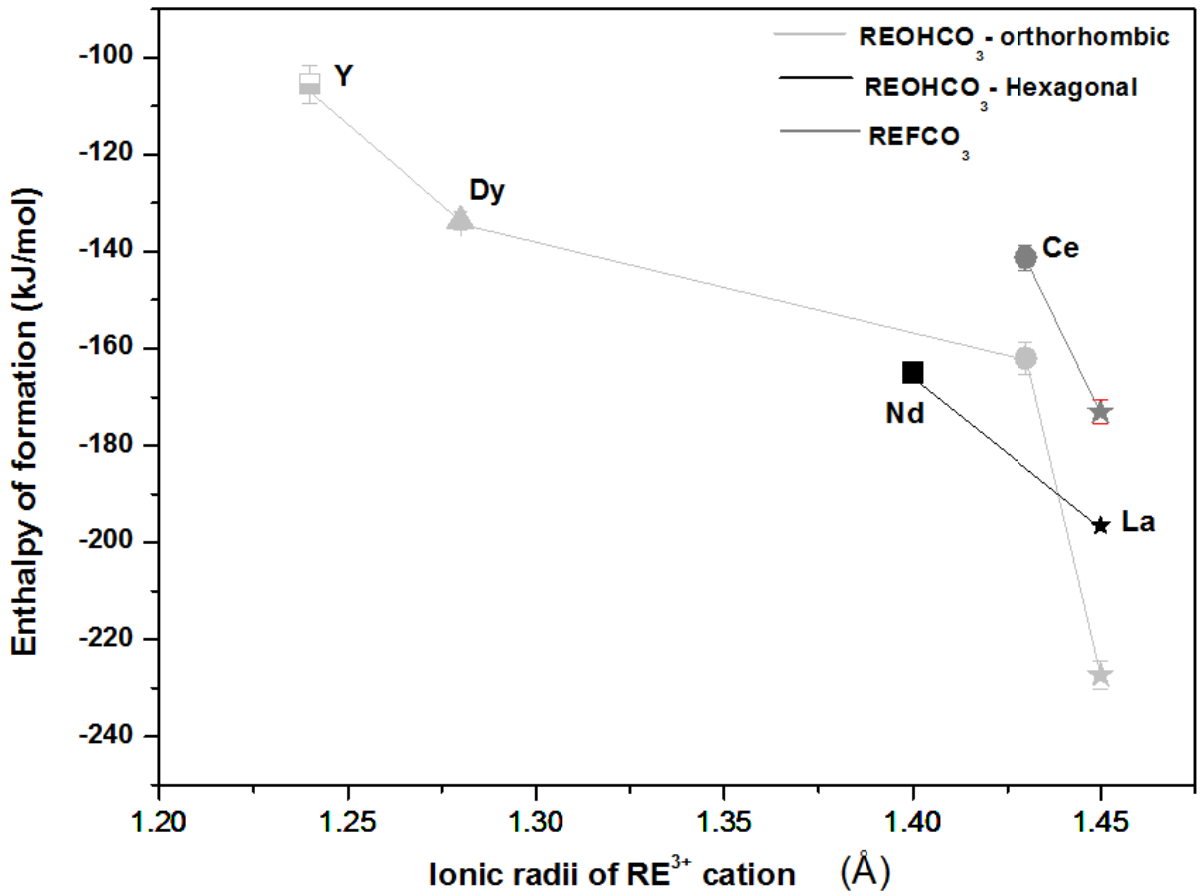


**Figure 3.** Enthalpy of formation of F/OH-bastnaesite as a function of ionic radii of $RE^{3+}$ cation

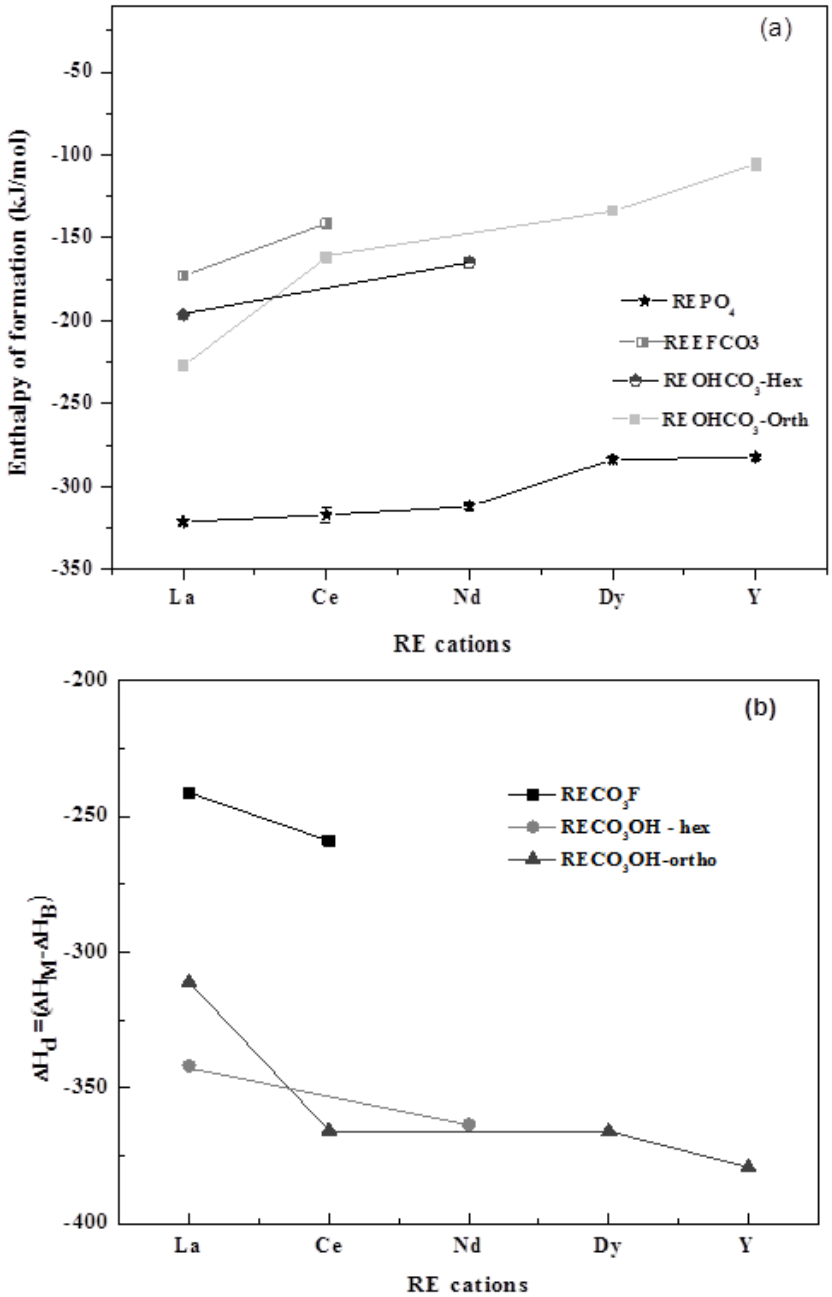


**Figure 4**. (a) A plot of enthalpy of formation values obtained for bastnaesite and monazite as a function of different RE. (b) a plot of difference in enthalpy of formation of bastnaesite and monazite for different REs